IEEE Access
Multidisciplinary | Rapid Review | Open Access Journal

Received May 3, 2020, accepted May 13, 2020, date of publication May 25, 2020, date of current version June 9, 2020.

Digital Object Identifier 10.1109/ACCESS.2020.2997254

From 2G to 5G Spatial Modeling of Personal RF-EMF Exposure Within Urban Public Trams

MIKEL CELAYA-ECHARRI[1], (Graduate Student Member, IEEE), LEYRE AZPILICUETA[1], (Senior Member, IEEE), JOLANTA KARPOWICZ[2], VICTORIA RAMOS[3], (Senior Member, IEEE), PEIO LOPEZ-ITURRI[4,5], (Member, IEEE), AND FRANCISCO FALCONE[4,5], (Senior Member, IEEE)

[1]School of Engineering and Sciences, Tecnologico de Monterrey, Monterrey 64849, Mexico
[2]Laboratory of Electromagnetic Hazards, Central Institute for Labour Protection—National Research Institute (CIOP-PIB), 00-701 Warszawa, Poland
[3]Telemedicine and e-Health Research Unit, Health Institute Carlos III, 28020 Madrid, Spain
[4]Department of Electric, Electronic, and Communication Engineering, Public University of Navarre, 31006 Pamplona, Spain
[5]Institute of Smart Cities, Public University of Navarre, 31006 Pamplona, Spain

Corresponding author: Leyre Azpilicueta (leyre.azpilicueta@tec.mx)

This work was supported in part by the School of Engineering and Sciences, Tecnologico de Monterrey, in part by the Ministerio de Ciencia, Innovación y Universidades, Gobierno de España (MCIU/AEI/FEDER,UE) under Grant RTI2018-095499-B-C31, in part by the Ministry of Science and Higher Education/National Centre for Research and Development and the Ministry of Family, Labour, and Social Policy, through the Poland National Programme Improvement of Safety and Working Conditions, and in part by Sub-Directorate-General for Research Assessment and Promotion, Spain, under Project PI14CIII/00056.

ABSTRACT The upcoming design and implementation of the new generation of 5G cellular systems, jointly with the multiple wireless communication systems that nowadays coexist within vehicular environments, leads to Heterogeneous Network challenging urban scenarios. In this framework, user's Radiofrequency Electromagnetic Fields (RF-EMF) radiation exposure assessment is pivotal, to verify compliance with current legislation thresholds. In this work, an in-depth study of the E-field characterization of the personal mobile communications within urban public trams is presented, considering different cellular technologies (from 2G to 5G). Specifically, frequency bands in the range of 5G NR frequency range 1 (FR1) and millimeter wave (mm-wave) bands within frequency range 2 (FR2) have been analyzed for 5G scenarios, considering their dispersive material properties. A simulation approach is presented to assess user mobile phone base station up-link radiation exposure, considering all the significant features of urban transportation trams in terms of structure morphology and topology or the materials employed. In addition, different user densities have been considered at different frequency bands, from 2G to 5G (FR1 and FR2), by means of an in-house developed deterministic 3D Ray-Launching (3D-RL) technique in order to provide clear insight spatial E-field distribution, including the impact in the use of directive antennas and beamforming techniques, within realistic operation conditions. Discussion in relation with current exposure limits have been presented, showing that for all cases, E-Field results are far below the maximum reference levels established by the ICNIRP guidelines. By means of a complete E-field campaign of measurements, performed with both, a personal exposimeter (PEM) and a spectrum analyzer within a real tram wagon car, the proposed methodology has been validated showing good agreement with the experimental measurements. In consequence, a simulation-based analysis methodology for dosimetry estimation is provided, aiding in the assessment of current and future cellular deployments in complex heterogeneous vehicular environments.

INDEX TERMS Radiofrequency electromagnetic fields (RF-EMF), Personal exposimeter (PEM), electromagnetic safety, e-field strength distribution, 3D ray launching (3D-RL), 5G, urban transportation trams.

I. INTRODUCTION

Tram systems are a popular public transportation service widely used in medium and large cities around the world [1]–[5]. Tram systems have limitation in the structure flexibility, as tramlines need fixed railways and overhead supplying cables supported by dedicated towers or mesh of lines fixed between nearby buildings. Nevertheless, they have several advantages when compared with other transportation vehicles such as small building cost, high passenger transport capacity, timeliness of service, safety, quiet, comfort and low environmental impact. In addition, owing to their use of

The associate editor coordinating the review of this manuscript and approving it for publication was Vittorio Degli-Esposti.

electric engines, they are zero-emission transportation systems and thus, are considered a pro-ecological public transport facility, which it is expected to have growing contribution to the entire transportation system in prospect years. However, Radio Frequency electromagnetic fields (RF-EMF) exposure assessments in urban tram transportation systems is challenging due to the presence of multiple EMF sources with their specific features, affectations and interrelations. In this context, realistic case studies are pivotal in order to achieve RF-EMF dosimetry impact evaluations of general public exposure in these complex heterogeneous environments. From a general approach, when discussing electromagnetic threats within the tram wagon cars, the low frequency component of exposure, which is created by the supplying network and electric engines, can be considered, as well as the high frequency components created by devices used inside the tram cars or entering from the sources used along the tram lines.

The low frequency components of EMF exposure are relatively weak, as trams use medium level of voltage in the supplying networks which do not cause high exposure to electric field nearby to be advised to be evaluated. Typical voltage used to supply trams is 3000 V, much less than the over 15 kV supplying local transformer station or the over 100 kV used to deliver electric power from electric power plants to local communities or enterprises. Additionally, because tram cars are lighter than trains, magnetic field exposure in trams is significantly lower than in trains [1]. Besides, electric currents supplying tram's engines are relatively weak, in the range of hundreds of amperes, with respect to the distance between overhead cables and passengers inside the tram cars or at tram stops platforms.

Conversely, high frequency electromagnetic field (HF-EMF) exposure inside a tram can be caused by different and multiple sources. On the one hand, EMF sources used inside the tram, such as RFID/NFC systems implemented in ticket machines and ticket counters, radiophones and trunking systems for tram drivers' use, mobile phones, wearables or other portable computers emitting signals in the GSM, UMTS and LTE systems up-link frequency bands, Wi-Fi facilities located inside the tram wagon cars to provide comfortable internet access for passengers, to cite the most common ones. On the other hand, EMF sources used along the tram lines, such as mobile phone base stations providing GSM, UMTS, LTE or 5G connections to the public radiocommunication networks, Wi-Fi facilities located in the city public space, nearby buildings or tram stops installations, public services communication facilities (police, firefighters, emergency, etc.), radio and television broadcasting antennas, mobile phones or other portable wireless devices used by people who stay nearby (at the tram stops, in parks, in outdoor bars or restaurants, etc.), among others.

Several studies in the literature have investigated the assessment of the RF-EMF exposure in different transportation vehicles and scenarios. In [6], the quantification of RF-EMF exposure for 18 public transport vehicles worldwide is presented. Conclusions indicate that, cellular up-link connections are in general not relevant when analyzing outdoor environments, but they play an important role as EMF sources in public transportation systems, exhibiting large variability. In another study from the same authors, [7], a monitoring protocol for RF-EMF measurements within different transportation vehicles was tested using portable devices. Their results showed that the up-link from mobile phones to base stations were the most significant radiation exposure within trains and trams, being the most significant values in trams. In addition, in [8], the representativeness of RF-EMF exposure measurements across different microenvironments, including different public transportation vehicles, is presented, showing that the highest mean total RF-EMF exposure is encountered usually near the central business district of the cities, whereas the lowest mean total exposure is encountered in the suburban residential areas of the cities. They present higher exposure levels within the trams than in the trains. This is explained by the fact that trams run mainly in or close to the central business district of the cities. Furthermore, [9] analyzes the RF-EMF exposure levels within a metro by means of frequency-selective exposimeters, concluding that the most significant levels of exposure were caused by mobile phones used by the passengers and local wireless Internet connections (Wi-Fi 2G). Other authors in [10], [11] assessed the impact in RF-EMF exposure within a train having a femtocell within the wagon infrastructure. They found that by connecting to a small cell, the brain exposure of the user could realistically be reduced by a factor 35 and the whole-body exposure by a factor 11. In another study by the same authors [12], the RF-EMF exposure due to the radiation originated by other people's devices within a train is assessed in a simulation study, showing that passive exposure from other passengers' mobile phones is not negligible and a femtocell within the train infrastructure could drastically reduce the total absorption for other users. Finally, the spatial characterization of personal RF-EMF exposure in public transportation buses is presented in [13], where worst-case studies considering different user densities and distributions for GSM, UMTS and LTE cellular communication systems were evaluated in terms of legislation compliance, showing that E-field levels were below the current established limits.

In contrast with the previous analysis, the aim of this work is to provide a comprehensive and intensive in-depth realistic case study of the personal mobile communications E-field spatial modeling considering different cellular technologies with special emphasis into future 5G up-link connections within complex heterogenous indoor environments, as urban transportation trams. For that purpose, and distinguishing itself from its predecessor [13], multiple factors must be carefully analyzed in order to provide RF-EMF assessment clear insight. Although both scenarios, the bus and the tram wagon car can be considered as complex indoor heterogeneous scenarios in terms of radio wave propagation, the metal structure influence of the tram as well as the supplying lines and towers, and specifically its presence in the city central

urban districts with huge passenger affluence, involves much more challenging propagation phenomena and thus presents higher exposure average levels. In this sense, all the HF-EMF components are subject of complex RF propagation distribution, with multiple reflections and absorptions due to the high density of clutter within the tram wagon cars, as well as the specific material properties of all the scatterers involved, based on the frequency under analysis. This specific behavior is particularly challenging for 5G scenarios together with the use of directive antennas at the UE side, emulating beamforming user case solutions, specially at high-frequency connection links over the millimeter wave (mm-wave) frequency band, as the ones presented in this work. Consequently, a deterministic simulation approach is presented in order to provide an efficient and accurate RF-EMF exposure assessment from microwave to mm-wave frequency bands, considering the specific morphology and topology of the tram wagon car, as well as different user densities within it, in real-case conditions. Fig. 1 presents a schematic view of the modelled tram crossing the city center of a typical city with special emphasis of the user mobile phone base station up-link and its RF-EMF exposure. In addition, a complete campaign of measurements is included in this work case study, performed with both, a personal exposimeter (PEM) and a spectrum analyzer within a real tram wagon car in realistic and controlled conditions, to precisely validate the proposed methodology.

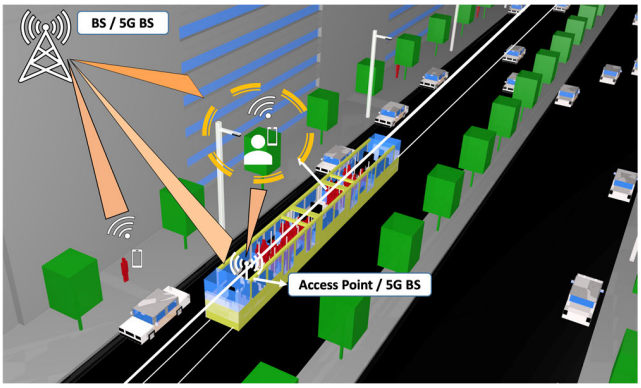

FIGURE 1. Schematic view of the modelled tram within a city and the mobile phone base station up-link which is focus this work.

This work is organized as follows: In Section II, a brief description of the current RF-EMF regulation is presented highlighting relevant 5G exposure studies. A complete description of the implemented campaign of measurements in the central business district tram route is explained in Section III, as well as the in-house deterministic methodology used for the EMF simulation of the tram scenario where different cellular technologies and user densities, have been considered. Section IV presents the simulation and measurement results for the different cellular technologies (from 2G to 5G), and discussion in relation with different exposure level thresholds. The ICNIRP limits used in the discussion of the results cover only considerations related to the thermal effects of RF-EMF exposure of regular human body. Besides, the proposed simulation methodology has also been validated in this section showing good agreement with the experimental measurements. Finally, conclusions are presented in Section IV.

II. REGULATION OF RF-EMF AND 5G EXPOSURE

With the next generation of cellular communication systems 5G, it is expected that the number of small cells will increase and will tend to be higher in crowded areas such as the central business district of the cities. To begin with, 5G systems have started to operate close to current cellular phone bands below 6 GHz or just below the mm-wave band (i.e., 28 and 39 GHz) in most of the countries around the world. Nevertheless, it is expected that future 5G systems will make higher use of the mm-wave band with frequencies that have not been used for cellular services. This will come with new concerns for compliance assessment for RF exposure limits. While new RF-EMF challenges arise from the deployment of 5G cellular networks is necessary to focus on basic restrictions and reference levels specific for the new frequency bands. Exactly as happens for legacy frequency bands, also for the bands dedicated to 5G, EMF regulations and legislation of most countries worldwide are based on (or are direct adaptations of) the guidelines of the International Commission on Non-Ionizing Radiation Protection (ICNIRP) [14], or the IEEE standard C95.1 developed by the IEEE International Committee on Electromagnetic Safety [15]. More relevant for a correct evaluation of the exposures due to 5G systems, is the identification of specific measurement techniques that allow to evaluate the real exposure due to this kind of signals, taking into account their specific technical characteristics (frame structure, up-link/downlink alternation, etc.). Going back to exposure limits, both ICNIRP Guidelines [14] and IEEE standards [15], have separate tiers for the occupationally exposed individuals and the members of the general public, with occupational limits being generally five times higher than those for the general public. A reduction factoris applied for the general publi limit definition in order to provide a more stringent restriction due to the fact that workers are exposed under known conditions and are trained to be aware of potential RF-EMF risks and to take appropriate precautions and mitigation measures – health and safety training program-while conversely that assumption cannot be expected for the general public. It must be remarked that these guidelines and standards are periodically revised and updated considering the new technological mplications for the RF-EMF exposure limitation based on the advantages concerning the health effects and potential health hazards made in the scientific knowledge. Accordingly, a revised version of these limits appeared in 2019 for the IEEE C95.1 2019 Standard [16] and for ICNIRP 2020 guidelines [17], recently published in March 2020. Several upgrades have been released in the new revised version of the ICNIRP 2020 guidelines but the most remarkable ones concerning the assessment of potential 5G exposure scenarios are briefly described below.

For what concerns whole body exposures reference levels should be averaged over a 30-minutes interval, while for local exposures reference levels should be averaged over a 6-minutes interval. With regard to localized exposures, ICNIRP Guidelines separate exposure longer than 6 minutes from exposure lasting less than 6 minutes, to protect against exposures due to non-continuous signals such as the ones produced by a 5G beamforming. Another important innovation introduced in the ICNIRP Guidelines concerns the fact that starting from the frequency of 2 GHz the reference levels are no longer defined in terms of E-field but in terms of power density, while previously the cut off occurred at 10 GHz. In general, the new aforementioned limits are expressed as a function of the frequency range, the exposure duration and also the spatial characterization. In this sense, specific limits and rules have been established in order to perform appropriate assessments in far field or near radiative/reactive scenarios. This aspect is a novelty introduced in ICNIRP Guidelines 2020 edition and had not been minimally considered in the previous editions which allowed to apply the rules defined for far field to all the exposure scenarios, leading to possible near field overexposures. Finally, specifications have been established to determine simultaneous exposure to multiple frequency fields situations with exposure additive effects due to heterogeneous networks environments. In Fig. 2 the general public -whole-body- E-field reference levels for the traditional and revised version of ICNIRP guidelines is presented, in which E-field levels between 0.1 MHz to 20 MHz are higher for the updated version [17], [18].

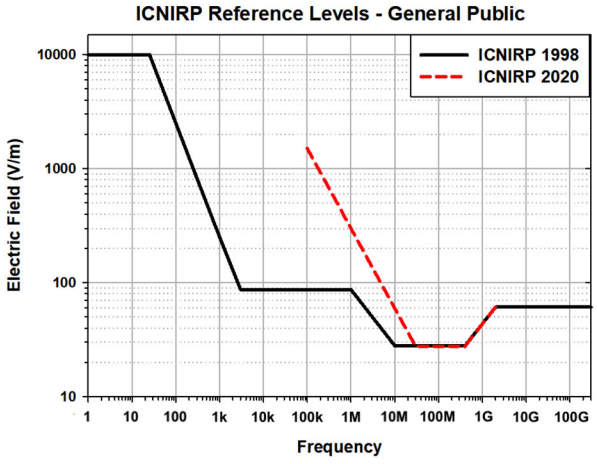

FIGURE 2. Comparison of ICNIRP reference levels for general public -whole body - between the original version (1998) and the revised version (2020).

There are different works in the literature which study the RF-EMF exposure of 5G User Equipment (UE) operating above 10 GHz. Zhao *et al.* [19], [20] assessed RF-EMF exposure compliance of phased arrays in mobile handset devices at 15 and 28 GHz frequency bands with respect to the Federal Communications Commission (FCC) regulations [21]. Thors *et al.* [22] present RF-EMF exposure evaluations in the frequency range 10-60 GHz for array antennas of UE and low-power radio base stations in 5G mobile communication systems to comply with the maximum permissible exposure limits specified by ICNIRP, IEEE and FCC. Moreover, Colombi *et al.* [23] present a complementary study regarding the output power levels of 5G devices above 6 GHz to comply with current EMF exposure limits.

As can be observed from the existing works, they mostly focus on the assessment of the RF-EMF exposure from 5G devices, but less attention is given to the EMF spatial characterization and the impact of radiation exposure that 5G handsets could have in the surrounding users, specifically within a microenvironment which can be densely populated. In general, it is expected that the transmitted power from the UEs will decrease at mm-wave frequency bands [24], [25]. Nevertheless, its constant abnormal pulse radiation can have health effects, along with the mode and duration of exposures. Reference [26] presents how some 5G signal characteristics, like the pulsing, could increase the biologic and health impacts of the exposure. Hitherto, it's worth noting that while there still isn't consensus on the scientific evidence in relation with potentially harmful effects of long-term exposure to RF-EMF, precautionary measures as well as further studies are called upon, especially considering the deployment of 5G networks [27] and the mm-wave frequency band, in particular [28]. In this sense, [29] presents a review of published literature between 2008 and 2018 of the relevance to radiofrequency radiation and health effects, corroborating lack of evidence of harmful health effects. In the same way, no clear evidence is concluded in a recent study analyzing the biological and health effects of RF-EMF exposures at the mm-wave frequency range (6–100 GHz), due to inconsistent relationships between exposure duration, intensity and the exposure effects [30]. Taken together, the epidemiological studies do not provide evidence of a carcinogenic effect of RF-EMF exposure at levels encountered in the general population. In summary, no effects of radiofrequency EMFs on the induction or development of cancer have been substantiated [31]. However, EMF research is still being promoted by WHO [32] to determine whether there are any health consequences from RF exposure levels.

III. MATERIALS AND METHODS

A. MEASUREMENT CAMPAIGN

A field exposure measurement campaign was designed and implemented within a real tram wagon car of the public transportation system of Bilbao, Spain, a medium-large size European city, with the aim of perform RF-EMF assessments in realistic-case conditions. Specifically, the empirical study purpose was to assess the main RF-EMF sources, with special emphasis into personal mobile communications, on this specific type of public transportation vehicle. Trams are commonly used by thousands of passengers every day worldwide and therefore, have huge potential to become future 5G deployments target environments. In this sense, tram routes developments usually connect the financial business

districts with the edges, crossing the cities centre, where there are naturally more people demand and thus, non-ionizing radiation exposure could increase. During the campaign of measurements, received E-field distribution levels have been obtained along the routes in order to assess compliance with legal exposure thresholds, respecting the usual routine of the trams.

Two different methodologies have been followed during the measurement campaign in order to provide clear insight in terms of use, performance and accuracy [13], [33]. For that purpose, a dynamic approach using a PEM device and a static procedure using a spectrum analyzer have been simultaneously performed to enable comparison.

The EME Spy Evolution personal dosimeter, from Microwave Vision SA – MVG (https://www.mvg-world.com/en), the newest released version of the EME Spy 121 previously used in [13], have been selected for the study, which is shown within the considered tram wagon car in Fig. 3. Specifically, the EME Spy Evolution is a portable measurement device which senses E-field strength over time, particularly updated for 5G scenarios allowing customized 5G frequency range user setups. The device can monitor up to 20 user-defined frequency bands for three different user-defined scenarios, which are the most commonly used frequency bands in Europe (EU), United States and Asia. For this study, the European scenario has been selected, with a sample rate of five seconds, which is the lowest allowed for this setup. The measured frequency bands for the EME Spy Evolution are summarized in Table 1.

FIGURE 3. EME Spy Evolution personal dosimeter used in the campaign of measurement placed within the tram.

In addition to the PEM measurements, a portable spectrum analyzer has been used in the measurement campaign in order to provide better accuracy, particularly over brief or irregular exposures. In this case, a Keysight N9912 Field Fox was selected, combined with two different antennas to fully cover the frequency range under analysis. The first one, dedicated to the current cellular networks' frequency bands: 900, 1800 and 2100 MHz (Dual band antenna PE51113-1 from Pasternack), and the second one for the 2.4 GHz frequency band

TABLE 1. Measured frequency bands of the EME Spy Evolution PEM.

Technology	Frequency (MHz)
FM	88 - 107
TV3	174 - 223
TETRA I	380 - 400
TV4&5	470 - 698
B28 (UL)	703 - 748
B28 (DL)	758 - 803
LTE 800 (DL)	791 - 821
LTE 800 (UL)	832 - 862
GSM+UMTS 900 (UL)	880 - 915
GSM+UMTS 900 (DL)	925 - 960
GSM 1800 (UL)	1710 - 1785
GSM 1800 (DL)	1805 - 1880
DECT	1880 - 1900
UMTS 2100 (UL)	1920 - 1980
UMTS 2100 (DL)	2110 - 2170
B40 TDD	2300 - 2400
WIFI 2G	2400 - 2483
LTE 2600 (UL)	2500 - 2570
LTE 2600 (DL)	2620 - 2690
WIFI 5G	5150 - 5850

(ECOM5-2400 from RS) typically used in wireless communications, such as Wi-Fi or Bluetooth, among others.

Non-ionizing radiation exposure measurements were performed in different days with high and low user density within the tram. The rush hour in a normal business day was chosen for high density, where the tram was almost full of people along all the route, while low density was measured when few people where inside the tram. In this sense, a single trip along the tram route has a duration of around 30 minutes. For the PEM measurements, two round trips were continuously evaluated for high and low population density. Conversely, spectrum analyzer measurements were performed only for the high-density case, during five minutes for each frequency band, emulating brief or irregular exposures (measurements shorter than 6 minutes are allowed, especially for 5G systems at mm-wave [17], [34]), normally given by dynamic personal mobile communications in complex heterogeneous environments as the considered tram wagon car. Results, legislation compliance and discussion of the measurement campaign are presented in Section IV.E.

Finally, a controlled measurement campaign was performed within an empty tram wagon car, just before the beginning of the route service, in order to verify and validate the proposed RF-EMF simulation technique. For that purpose, a transmitter antenna, connected to a signal generator at 2.4 GHz was located at the right part of the wagon tram at 1.1 m height with a transmission power of 10 dBm. The selected antennas were ECOM5-2400 from RS, both omnidirectional. The employed signal generator was a portable N1996A unit, from Keysight Technologies, and the spectrum

analyzer was a Keysight N9912 Field Fox. Measurements were performed with 100 MHz bandwidth at 2.4 GHz frequency with a measurement time at each considered point of 60 seconds. The E-field exposure level per location has been calculated from the measured received power considering the antenna factor, with the following formula [35]:

$$E = P_R - P_{gain} + L_{cable} + AF \tag{1}$$

where E is the E-field level in V/m, P_R is the received power in dBm, P_{gain} is the preamplifier gain, and AF is the antenna factor of the receiving antenna. Results, validation and discussion of the controlled measurement campaign are presented in Section IV.F.

B. RAY LAUNCHING TECHNIQUE

With the aim of analyzing the impact of non-ionizing radiation exposure for each passenger within the complete volume of the tram wagon car, an in-house deterministic 3D Ray Launching (3D-RL) technique has been used. The algorithm is based on Geometrical Optics (GO) approach and the Uniform Theory of Diffraction (UTD). RL approaches basis establish a set of rays which go through a path from the transmitter to the receiver, considering geometric specifications and geometrical optics principles as well as their corresponding electromagnetic phenomena such as reflection, refraction and diffraction. By means of a site-specific description of the propagation environment, the complex impulse response with the complete channel information can be obtained. Moreover, the electric field E created by GO and the diffracted electric field created by UTD are calculated by [35]:

$$E_{GO}^{\perp\parallel} = \sqrt{\frac{P_{rad} D_t(\theta_t, \emptyset_t)\eta_0}{2\Pi}} \frac{e^{-j\beta_0 r}}{r} \mathrm{X}^{\perp\parallel} L^{\perp\parallel} \tag{2}$$

$$E_{UTD}^{\perp\parallel} = e_0 \frac{e^{-jks_1}}{s_1} D^{\perp\parallel} \sqrt{\frac{s_1}{s_2(s_1+s_2)}} e^{-jks_2} \tag{3}$$

where $\beta_0 = 2\pi f_c \sqrt{\varepsilon_0 \mu_0}$, $\varepsilon_0 = 8.854{*}10^{-12}$ F/m, $\mu_0 = 4\pi{*}10^{-7}$H/m and $\eta_0 = 120\pi$ ohms. P_{rad} is the radiated power of the transmitter antenna, $D_t(\theta_t, \emptyset_t)$ is the directivity, $\mathrm{X}^{\perp\parallel}$ and $L^{\perp\parallel}$ are the polarization ratio and path loss coefficients for each polarization, r the distance in the free space and f_c the transmission frequency. In equation (3) , $D^{\perp\parallel}$ are the diffraction coefficients for each polarization and s_1, s_2 are the distances from the source to the edge and from the edge to the receiver point. It has been stated in the literature that the basis of GO/UTD predicts accurately wireless communication propagation when a complete 3D scenario is taken into account [36], being the main drawback its high computational cost. Thus, in order to reduce the computational load of the presented algorithm, hybrid techniques have been proposed combining the RL approach with different methods, such as Neural Networks (NN) [37], Diffusion Equation (DE) [38] or Collaborative Filtering (CF) [39]. These hybrid methods achieve precise results whilst reducing the computational cost, leading to an Optimized 3D-RL approach, more efficient and robust for complex scenarios.

The 3D-RL tool is based on a modular structure, where different libraries can be integrated. In reference [13], a novel electromagnetic safety analysis module implemented in the 3D-RL algorithm for the analysis of non-ionizing radiation exposure has been presented and validated within a vehicle at frequencies below 6 GHz. In this work, a further step is proposed, providing the development of an extension of the electromagnetic safety analysis module for the RF-EMF exposure assessment at mm-wave frequencies. In this sense, different electric conductivity and relative permittivity models for the 1-100 GHz frequency range, obtained by the Recommendation ITU-R P2040-1, [40], have been added to the new implemented mm-wave electromagnetic safety module. Although the previous version of the 3D-RL tool enabled the insertion of simplified human body models [13], [41], new upgrade implementations have been included, considering the different skin dielectric properties and the dispersive behavior of its components, at the mm-wave frequency range. In addition, special attention has been given to the atmosphere absorption phenomena, which is more relevant at higher frequencies [42]. Finally, different beamforming capabilities are also included, leading to multiple types of antennas' analyses considering directional and adaptive radiation patterns, as the employed in 5G systems. Fig. 4 presents the schematic view of the Optimized 3D-RL simulation methodology for RF-EMF radiation exposure assessment where both modules for electromagnetic safety analysis at micro-wave and mm-wave frequency bands, are presented.

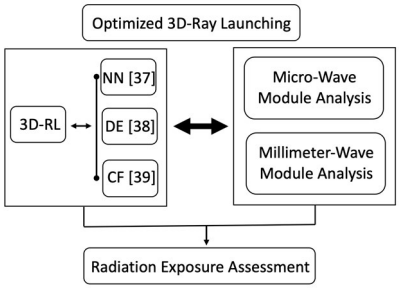

FIGURE 4. Modular structure of the optimized 3D-RL approach.

It is important to clearly state that the RL approach provides an uncertainty near field results area in the vicinity of the transmitting antenna, which has not been considered in the presented work. Thus, an exclusion area of 5λ around the transmitter antenna has been considered in order to avoid near field results [35].

C. SCENARIO DESCRIPTION

A collage of real images of the tram wagon car considered for simulation as well as for the measurement campaign, is presented in Fig. 5. The internal or indoor distribution of the tram is depicted, where the different seats and handholds can be seen, as well as the metallic bouncy structure.

The same scenario has been implemented in the 3D-RL simulation software, to assess radiation exposure within the complete volume of the vehicle, in realistic-case conditions.

FIGURE 5. Real wagon tram car used in the campaign of measurements and internal distribution of the vehicle.

For that purpose, the same dimensions and geometry of the tram wagon car have been considered, taking into account all the dispersive material properties of all the obstacles within it, with their corresponding conductivity and relative permittivity at the frequencies under analysis. In addition, simplified human body models have been introduced in the tram emulating high and low-density scenarios, in order to have insight of the user density effects over the E-field distribution within the vehicle. Specifically, 101 passengers have been considered for the high-density case and 33 passengers for the low-density case. In Fig. 6, both tram wagon cars scenarios, created for the 3D-RL simulation tool, are presented.

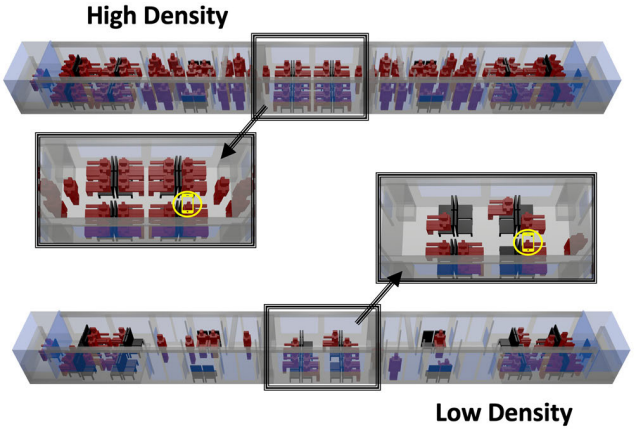

FIGURE 6. Simulated tram wagon car scenarios with different user densities.

Multiple simulations have been performed emulating a seated person (TX locations are depicted in Fig. 6 with a yellow smartphone icon) making phone calls using different mobile communication systems. By means of these simulation results, E-field distribution levels have been obtained for the complete 3D scenario. The summary of the different simulation case studies with their corresponding features, are presented in Table 2.

TABLE 2. Description of cases considered for simulation.

Cases	System	Frequency (MHz)	Antenna	Users Density
Case I	2G/3G	900	Omnidirectional	High / Low
		1800		
		2100		
Case II	4G	800	Omnidirectional	High / Low
		1800		
		2600		
Case III	5G	700	Omnidirectional	High / Low
		3700		
Case IV	5G	3700	Directional	High / Low
		26000		

It must be remarked that two different approaches have been followed for the 5G system case. The first one considering an omnidirectional antenna at the UE, for two frequency bands below 6 GHz (700 and 3700 MHz frequency bands). These frequency bands have been chosen as they are the 5G systems allocated bands below 6 GHz in Spain [43]. The second approach, considering a directional antenna in the UE in order to analyze 5G systems radiation exposure from the handset. Albeit there is a limited amount of commercial cellular networks that use beamforming in the UE for 5G systems, some examples can be encountered for mm-wave bands [44]. In the literature, several works propose novel multiple-input-multiple-output (MIMO) antennas for the 5G mobile handsets. Some of them are for mm-wave bands, such as the work presented in [45], which proposes a novel architecture distributed phased arrays based MIMO (DPA-MIMO) for 5G mm-wave cellular UE, and [46], which presents a cost-effective mm-wave cellular-Wi-Fi design methodology based on the new DPA-MIMO architecture. In addition, other works presents novel MIMO antennas for 5G mobile devices at frequency bands below 6 GHz, such as [47], which presents a low-profile wideband antenna for the MIMO application of 5G mobile handsets in the 3.3 GHz to 3.8 GHz frequency band. Overall, works presented in [47]–[50] introducing novel antennas for the 5G MIMO application of mobile devices and concluding that all their features make them suitable to be applied in 5G mobile devices as MIMO antenna element. Due to the fact that many works have proposed the use of beamforming in the future 5G mobile handsets, this relevant case has been considered. Therefore, in Case IV (see Table 2 for reference), directional antennas have been used at 3700 MHz and 26 GHz frequency bands, to analyze radiation exposure for 5G systems which can use beamforming at the UE.

Finally, the input simulation parameters employed for the realistic-case study, are shown in Table 3.

IV. RESULTS AND DISCUSSION

A. 2G/3G/4G CELLULAR SYSTEMS

In this section, the comparison of E-field exposure levels as a function of user distribution within the complete volume of the tram, has been obtained for 2G/3G/4G cellular communication systems.

TABLE 3. Parameters for the 3D-RL simulations.

Simulation Selected Parameters		Ref.
Frequency of operation (MHz)	See Table 2	
Transmitted power level	10 dBm	[22-23]
Tx / Rx Gain	0 dB	
Antenna Type	See Table 2	
Horizontal angular resolution (ΔΦ)	π/180 rad	[51]
Vertical angular resolution (Δθ)	π/180 rad	[51]
Permitted maximum reflections	6	[51]
Angular resolution Diffracted rays	π/20 rad	[52]
Cuboids size	10 cm	

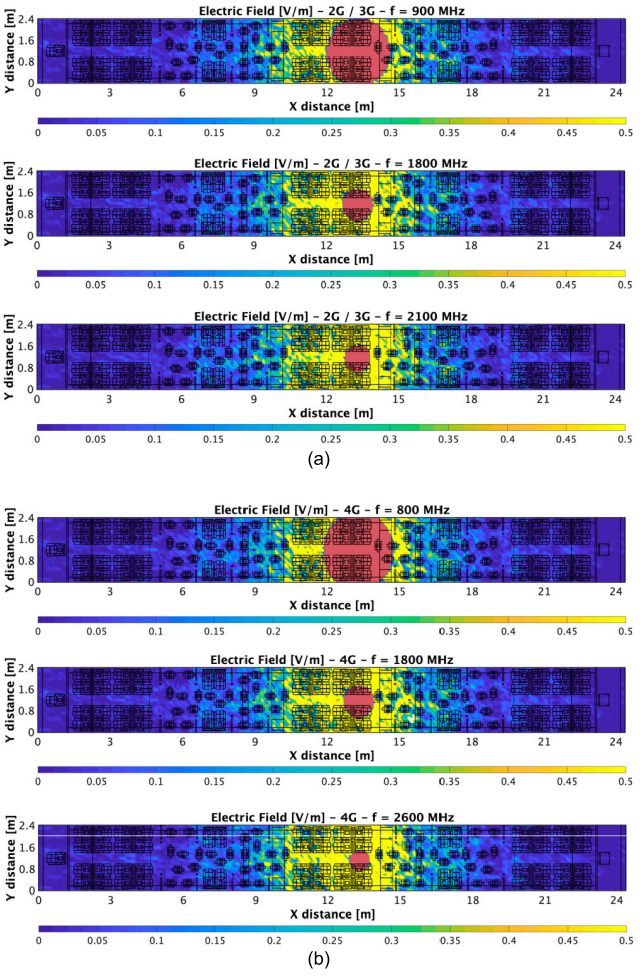

FIGURE 7. Comparison of the simulated E-field exposure levels within the tram for the high-density case. The transmitter is placed in the middle of the tram with 10 dBm transmitting power. 5λ m exclusion area around the transmitter has been considered in order to avoid near field results, (a) 2G / 3G cellular systems (b) 4G cellular systems.

Fig. 7 presents the E-field levels comparison considering the different frequency bands allocated for 2G/3G cellular systems (900, 1800 and 2100 MHz) and for 4G cellular systems (800, 1800 and 2600 MHz), for the high-density case within the tram. The cut planes correspond with the same height as the transmitter is placed, in this case 1.3 m height, emulating a seated passenger making a phone call, placed in the middle of the tram. From the results, the highest E-field distribution levels are concentrated in an area of approximately 2 – 2.5 m around the transmitter antenna (see yellow results in the graphs), whereas a significant reduction is observed in the rest of the tram's volume. The distribution behavior trend is consistent for all the high-density study cases where the body shielding effect of the nearby passengers can be clearly observed, following the body shielding hypothesis of worst-case scenarios presented in [13]. Note that the considered exclusion area for each frequency case has been 5λ in order to avoid uncertainty near field results (red area in the graphs). This leads to a larger exclusion area at lower frequencies, as it can be observed in Fig. 7.

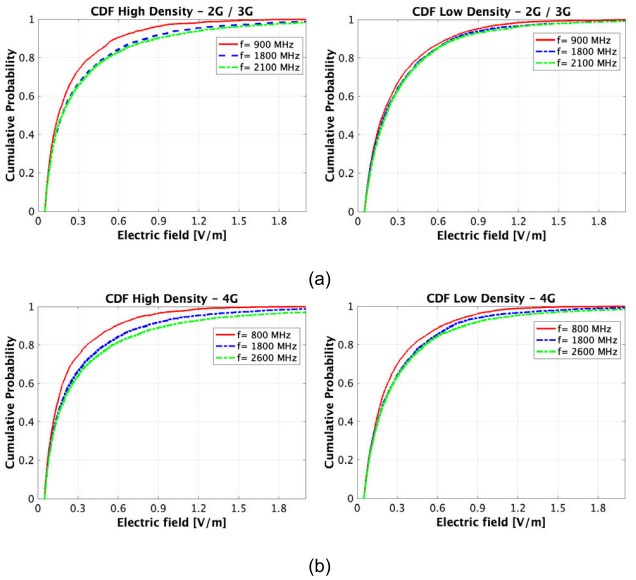

FIGURE 8. CDF of E-field average exposure values for different users' densities within the complete volume of the tram at different frequencies, (a) 2G/3G cellular systems (b) 4G cellular systems.

To have clear insight into the differences of E-field distribution values for the different users' densities, Fig. 8 presents the E-field cumulative distribution probability (CDF) for 2G/3G systems frequencies (Fig. 8a) as well as for 4G systems (Fig. 8b), considering the far field results of the complete volume of the tram. When low-density cases are considered, higher levels are clearly obtained in the E-field CDF graphs due to a uniform E-field distribution with negligible body shielding affectation. Nevertheless, an opposite distribution behaviour is presented for high-density cases, due to higher signal concentrations in the impact areas, reducing E-field levels in the rest of the tram. Consequently, high-density CDFs present lower values than low-density cases for both analyzed cellular technologies.

These results show the importance of analyzing E-field exposure, considering different non-ionizing radiation areas, determined by different user densities, as it is presented in [13]. In this sense, a summary of the E-field average levels per area, for all the considered 2G/3G/4G systems' frequency bands, is presented in Table 4. The impact and

TABLE 4. E-field average results comparison per areas considering different users' densities at 2G/3G/4G cellular systems' frequency bands.

	2G / 3G E-field Average (V/m)					
	900 MHz		1800 MHz		2100 MHz	
Areas	HD	LD	HD	LD	HD	LD
Impact Area ($5\lambda - 1.5$m)	NF*	NF*	0.99	0.94	1.04	0.95
Impact Area ($5\lambda - 2$m)	0.93	0.99	0.82	0.80	0.85	0.81
Impact Area ($5\lambda - 2.5$m)	0.78	0.87	0.70	0.71	0.72	0.71
Remote Area	0.07	0.14	0.06	0.13	0.06	0.13
	4G E-field Average (V/m)					
	800 MHz		1800 MHz		2600 MHz	
Areas	HD	LD	HD	LD	HD	LD
Impact Area ($5\lambda - 1.5$m)	NF*	NF*	0.99	0.94	1.18	1.09
Impact Area ($5\lambda - 2$m)	0.99	0.92	0.82	0.80	0.95	0.90
Impact Area ($5\lambda - 2.5$m)	0.83	0.83	0.70	0.71	0.80	0.79
Remote Area	0.06	0.14	0.06	0.13	0.06	0.13

NF* = Near Field; HD = High Density; LD = Low Density

remote areas are represented in different colours for a better comprehension (see Fig. 9 for reference).

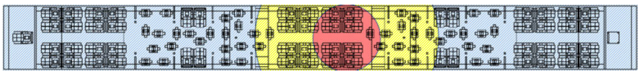

FIGURE 9. Representation of impact and remote area within the complete volume of the tram. Near-field exclusion area colored in red.

From the data results, both areas can be precisely determined, leading to an impact area definition of 2.5 m from the transmitter location. For all high-density cases under study, comparison shows higher E-field average levels in the impact areas, due to body shielding effects. In accordance, the difference is raised at higher frequency bands, as the analyzed area is bigger than the one at lower frequencies, where the near field exclusion area is larger. On the other hand, significantly low E-field exposure levels are obtained in the remote area for all the analyzed case studies. Therefore, user density as well as the frequency under analysis play a key role for the spatial characterization of E-field exposure assessment in complex indoor vehicular environments.

Some relevant conclusions can be stated, analyzing in deepness and comparing these results with the previously presented in [13]. Although completely different approaches have been followed in both works, worst-case versus realistic-case studies, same E-field distributions patterns are presented for the different user-density considered scenarios. In contrast, new obtained E-field radiation results are significantly lower than those presented in [13], where the worst-case scenario was considered. Finally, it must be remarked that these new obtained E-field average levels are consistent with the ones measured in different vehicles' measurement campaigns from the literature [53].

B. TOWARDS 5G CELLULAR SYSTEMS

The design and implementation of commercial 5G cellular systems, has already began in many countries worldwide, leading to the next generation of wireless communication systems. This new generation is expected to address the mm-wave frequency range in order to provide high data rate and low latency communications. Nevertheless, future 5G deployments will be challenging, due to the severe channel impairments at the mm-wave frequency range. As a consequence, the first 5G cellular systems' deployments in EU have been allocated in known and controlled frequency bands below 6 GHz, such as 700 MHz and 3700 MHz. In this section, a complete realistic-case study for current and future 5G deployments in complex indoor environments, is presented. For that purpose, two different types of antennas have been considered in the 5G mobile handset: an omnidirectional antenna for the 700 and 3700 MHz frequency bands, and a directive antenna with beamforming for the 3700 MHz and 26 GHz frequency bands (see Table 2 for further information).

In Fig. 10 and Fig. 11 the bi-dimensional planes representing the E-field exposure levels for the omnidirectional antenna case at 700 and 3700 MHz, respectively, are depicted.

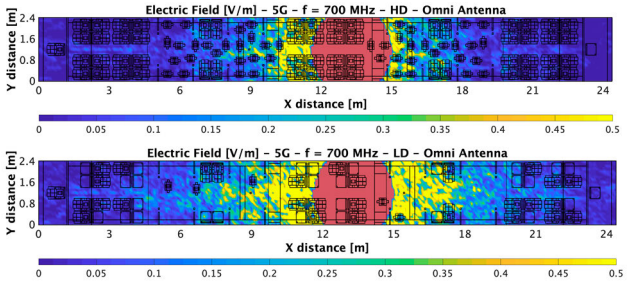

FIGURE 10. Comparison of the simulated E-field exposure levels within the tram at 700 MHz frequency band for different users' densities. The transmitter is placed in the middle of the tram with 10 dBm transmitting power. 5λ m exclusion area around the transmitter has been considered in order to avoid near field results.

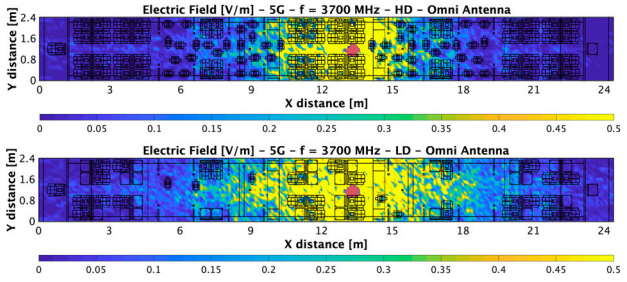

FIGURE 11. Comparison of the simulated E-field exposure levels within the tram at 3700 MHz frequency band for different users' densities. The transmitter is placed in the middle of the tram with 10 dBm transmitting power. 5λ m exclusion area around the transmitter has been considered in order to avoid near field results.

Comparing the obtained 5G results with the previous analyzed cellular systems, the same trend is obtained, showing consistent E-field spatial distribution. Higher exposure levels for well-defined impact areas are presented in high-density scenarios. On the other hand, more heterogeneous

TABLE 5. Comparison of E-field average values per different areas and users' distribution for the different analyzed frequency bands in 5G cellular systems with omnidirectional antennas.

	E-field Average (V/m)			
	F = 700 MHz		F = 3700 MHz	
Areas	HD	LD	HD	LD
Impact Area (5λ – 1.5m)	NF*	NF*	1.19	1.13
Impact Area (5λ – 2m)	NF*	NF*	0.97	0.96
Impact Area (5λ – 2.5m)	0.69	0.76	0.82	0.84
Remote Area	0.07	0.15	0.06	0.13

NF* = Near Field; HD = High Density; LD = Low Density

distribution is presented in the transition between the impact areas and the remote areas in low-density cases, leading to diffuse or not well-defined areas' determination, due to less body shielding effect. Moreover, the frequency-dependency impact is observed in signal propagation, giving rise to higher exposure values at lower frequencies, as signal absorption by scatterers is lower. In Fig. 12, the E-field exposure CDF for the complete volume of the tram is presented, to provide clear insight into the differences between both 5G frequencies and user densities, considering an omnidirectional antenna.

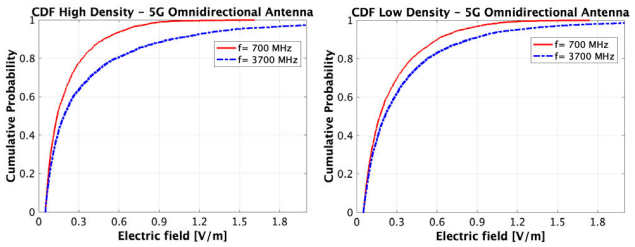

FIGURE 12. CDF of E-field average exposure values for different users' densities within the complete volume of the tram at different frequencies below 6 GHz of 5G cellular systems.

Analyzing in deepness the CDFs results, the body shielding hypothesis arises as in previous studies, showing higher exposure levels for the low-density cases, when the complete volume of the scenario is considered. Therefore, it can be stated that the evaluation of the body shielding effect is pivotal when the impact area is analyzed, but the effect is absorbed by the remote areas' average levels, when the whole scenario distribution is considered.

In Table 5, a summary of the average E-field values per area is presented, considering different ranges from the transmitter location. For all cases, comparisons are provided, showing the differences between high and low-density cases, and the significant E-field exposure decay at the transition between the impact area and the remote area.

In order to provide clear insight into the beamforming effects on 5G mobile handsets' scenarios at frequency bands under 6 GHz and also in mm-wave, simulations emulating 5G smart-phones' MIMO systems have been performed, using the simulation parameters previously presented in Table 3. Directional links have been simulated establishing communication with a 5G small cell within the tram, in order to assess radiation exposure within the volume of the antenna beams. A relevant research case study has been chosen for the transmitter antenna beam direction, where line of sight is presented in the low-density case but not in high-density, allowing comparison. However, it must be remarked that all type of scenarios and beam direction case studies for directive antennas can be evaluated, using the inhouse deterministic 3D-RL simulation technique proposed in this work.

Fig. 13 and Fig. 14 presents the XZ bi-dimensional planes of E-field radiation exposure levels for both user densities, emulating a seated person (TX height = 1.3 m) making a phone call within the tram, at 3700 MHz and 26 GHz frequency bands, respectively.

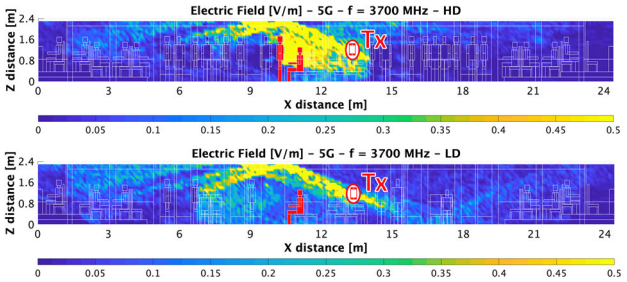

FIGURE 13. Comparison of the simulated E-field exposure levels within the tram at 3700 MHz frequency band for different users' densities. The transmitter is located in the middle of the tram with 10 dBm transmitting power and a directional radiation pattern.

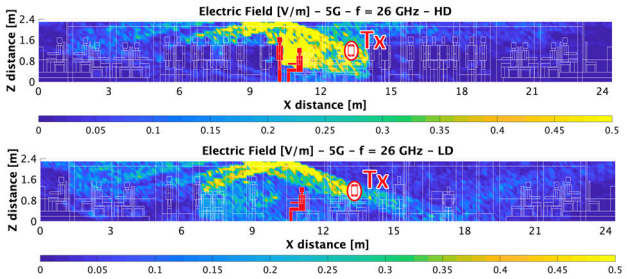

FIGURE 14. Comparison of the simulated E-field exposure levels within the tram at 26 GHz frequency band for different users' densities. The transmitter is located in the middle of the tram with 10 dBm transmitting power and a directional radiation pattern.

From the comparison, important body shielding effects can be clearly observed in the high-density case, at both frequency bands. As expected, the standing person within the beam, blocks and concentrates the signal in the impact area, leading to higher local radiation exposure levels over the seated person (see stand and seated passengers, in red, in Fig 13 and Fig. 14). Otherwise, a homogeneous directive E-field distribution behaviour is presented in the low-density case, due to a lack of body shielding effects, allowing significantly less exposure over the same seated passenger. In Fig. 15, radiation beams' CDFs are depicted, to analyze in deepness the E-field distribution levels for the corresponding 5G directive communication links.

Obtained graphs are notably different than the previous analyzed cases, showing higher exposure values, as only the

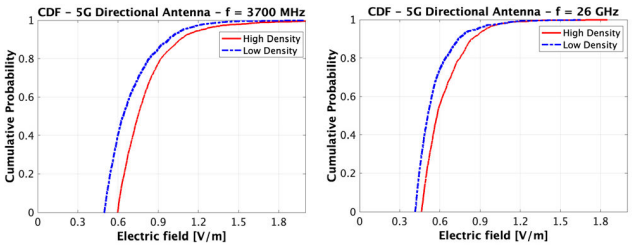

FIGURE 15. CDF of E-field average exposure values for different users' densities within the beam of the 5G directional antenna at 3700 MHz and 26 GHz frequency bands.

TABLE 6. Comparison of E-field average exposure values over passengers considering different users' distributions at 5G cellular systems frequency bands with omnidirectional antennas.

	E-field (V/m)			
	F = 3700 MHz		F = 26 GHz	
	HD	LD	HD	LD
Standing Person				
Head	1.17	N/A*	0.91	N/A*
Chest	0.99	N/A*	0.77	N/A*
Seated Person				
Head	0.76	0.32	0.60	0.26
Chest	0.65	0.13	0.53	0.10

NA* = Not Applicable; HD = High Density; LD = Low Density

spatial points of the beam are considered. Besides, the user density trend is consistent at both frequencies, with lower exposure levels in the low-density cases, due to the body shielding influence. Consequently, a further E-field exposure analysis is provided considering the body shielding effects over passengers located within the radiation beams of the directive antennas. In Table 6, the E-field exposure values at the surface of the head and chest of the stand and seated passengers, are summarized (see red passengers in Fig. 13 and 14 for reference). The highest E-field exposure levels are obtained in the head and chest of the standing person, who is acting as a shield, concentrating the signal. Moreover, a slightly difference between E-field levels is presented for both frequency bands, with higher exposure values at lower 5G frequencies, due to higher signal losses in the mm-wave range.

C. 2G/3G/4G/5G EMF COMPARISON

In this section, RF-EMF statistical comparisons are presented for all the cellular communication systems under analysis, in terms of E-field distribution within the tram wagon car. For that purpose, an in-house procedure has been developed using MATLAB's statistical libraries and functions to process the simulation results. For each cellular technology, different case studies are represented considering high and low-density scenarios as well as their corresponding frequency bands and types of transmission antennas. The boxplot graphs showing the maximum E-field levels, the median value and the 25th and 75th percentiles for each analyzed case are depicted in Fig. 16. It must be remarked that all the statistical results have been obtained considering only E-field levels in the far field region, and therefore, respecting the 5λ exclusion area from the transmitter location [35]. Several relevant aspects are worth commenting, analyzing the results from Fig. 16:

- For all the analyzed 2G/ 3G, 4G and 5G cellular communication systems, considering an omnidirectional transmitting antenna (Case I, II and III), the presented boxplots correspond to the E-field exposure levels for the complete volume of the tram wagon car. E-field results exhibit slight variations depending on the frequency under analysis, but the maximum E-field levels are obtained for the high-density cases, at all frequencies considered (around 1 V/m).

Conversely, E-field median values are higher for the low-density cases at all analyzed frequencies, because the remote area is larger than the impact area, when the full volume of the vehicle is considered. The obtained median E-field values are around 0.2 V/m approximately.

- Focusing on 5G systems (Case III and IV), notable differences can be observed when considering an omnidirectional or a directive antenna in the UE. In that sense, when considering the complete volume of the tram wagon car, Case III and Case IV (left), E-field levels are significantly lower for the directive antenna case.

The comparison shows a significant 60% E-field decrease, with maximum exposures levels falling from, approximately 1 V/m in the omnidirectional case, to 0.4 V/m in the directive case. This drop-down behavior can be explained by the different antennas' radiation patterns. In other words, when considering a directive antenna, the radiation pattern is aligned in its incident direction, allowing less non-ionizing radiation over the rest of the vehicle, which in average leads to lower E-field levels when the complete volume is assessed.

- Nevertheless, the opposite trend can be observed in Case IV (right), where the E-field boxplot results are representing only the radiation exposure levels within the directive connection beam. Analyzing this particular case study, the maximum and median values are much higher than in the previous analyzed cases, approximately around 1.1 V/m and 0.75 V/m, respectively. In general, an accurate characterization of this specific E-field distribution behavior is pivotal to predict in advance the RF-EMF behavior of future 5G cellular systems at the mm-wave frequency range, where brief or irregular local exposure assessment will be required due to massive directive communication links, generated by 5G MIMO antennas.

- RF-EMF compliance evaluation must be performed assuming the worst-case conditions but, in this work, a realistic approach is provided, where all the obtained E-field exposures levels are far below the current limits and thus, showing compliance with current international EMF regulation. Specifically, maximum E-field peaks achieved (see Fig. 16 for reference) do not exceed the 1-2% of the ICNIRP corresponding established limits per frequency, considering a transmission power of 10 dBm, which is a typical value for current mobile handsets as well as for future 5G-specific

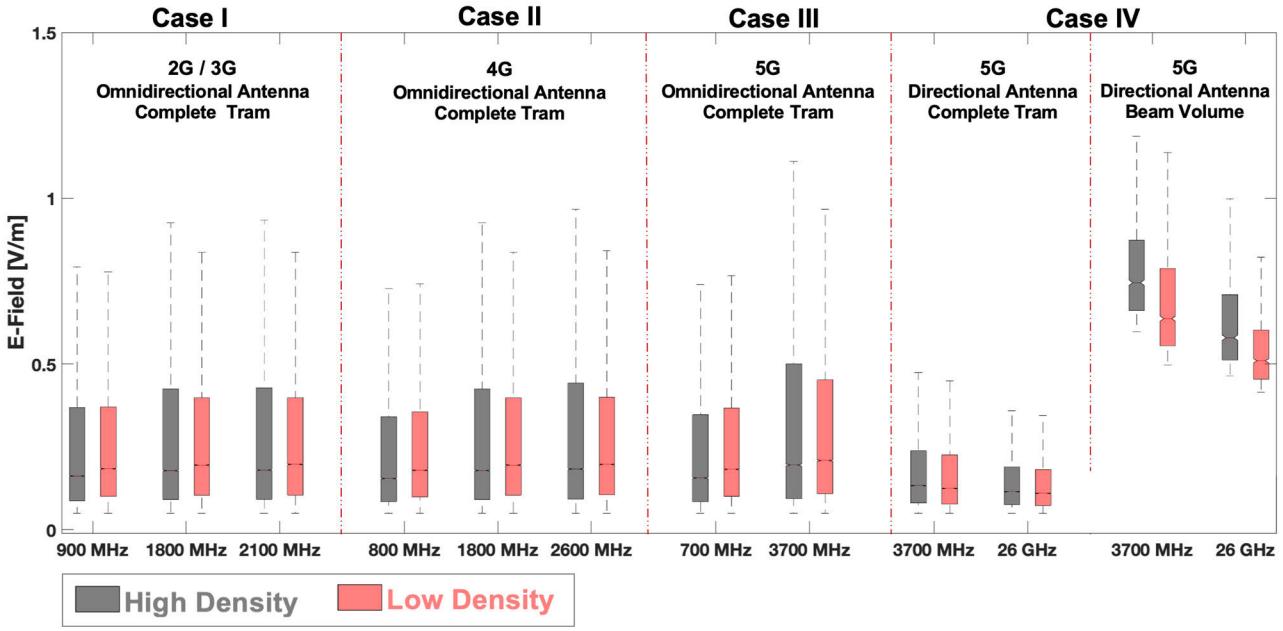

FIGURE 16. Boxplot comparison of E-field average exposure values for the different mobile communication systems and different users' densities.

smart phones [22], [23], [54], [55]. However, albeit the obtained E-field levels present compliance with current EMF legislation, it is important to emphasize that multiple aspects, such as the users' density within the tram wagon car or the radiation pattern of the transmitter antenna, can lead to different E-field distributions over the exposure areas, where other passengers can be exposed to higher radiation without knowing about it.

D. MEASUREMENT RESULTS

In this section, the measured RF-EMF exposure levels for both, the dynamic (PEM devices) and the static (spectrum analyzer) campaign of measurements' methodologies, are presented. For both approaches, a high-density case was considered in the morning rush hours and a low-density case during the off-peak hours, in order to compare EMF exposure levels with different users' densities. A further description of the procedure and the specific features of the measurements campaign, can be found in Section III.A.

It's worth noting that the use of PEMs has been increasingly used for dynamic exposure assessment in epidemiological research [56]–[58]. However, less research on the measurement accuracy of these devices is available in the literature. Multiple factors such as the scenario's complexity, the measurement procedure application or the device's physical location can affect PEM measurements. But one of the most significant for complex indoor environments as the tram wagon car scenario presented in this work, is due to the human body influence and/or the human body shielding effects [13], [59], [60], which can lead to severe underestimations than can reach up to a factor of two [61]. Hence, the measurement technique is pivotal in order to reduce or mitigate possible underestimation during PEM measurements campaigns. Thus, measurements were carried out with the PEM device in the vicinity of the body, but not directly on the body, following a validated and reliable PEM measurement procedure [13], [62]. For both user densities, the EMF exposure results obtained using PEM devices, are depicted in Fig. 17.

From these results, it can be observed that the highest E-field levels are produced by mobile communication systems (GSM/UMTS) in the high-density case (which corresponds with a 9.45% of the lowest reference level provided by ICNIRP guidelines for the corresponding frequency band (41.25 V/m)), and on the other hand, the highest E-field levels are produced by Wi-Fi 2G systems, in the low-density case (4.92% of the lowest reference level provided by ICNIRP guidelines for the corresponding frequency band (61 V/m)). Moreover, relevant exposure peaks are obtained in both analyzed cases from personal up-link mobile communications (marked in the figure).

As it has been introduced, PEM measurements must be analyzed carefully in terms of precision and reliability. In this sense, uncertainty of the measurement accuracy of PEM devices has been investigated before [59], [63], [64]. Therefore, a static approach using a spectrum analyzer has also been followed in the campaign of measurements, to contribute and to provide more detail and rigor to this work. In Fig. 18, 19, 20 and 21, the E-Field, power and spectrogram values at different frequency bands (GSM/UMTS 900, UMTS 2100, GSM 1800 and WIFI 2G) are presented, considering brief exposure in a high-density scenario with realistic-case conditions. It must be pointed out that E-field levels have been obtained applying the corresponding

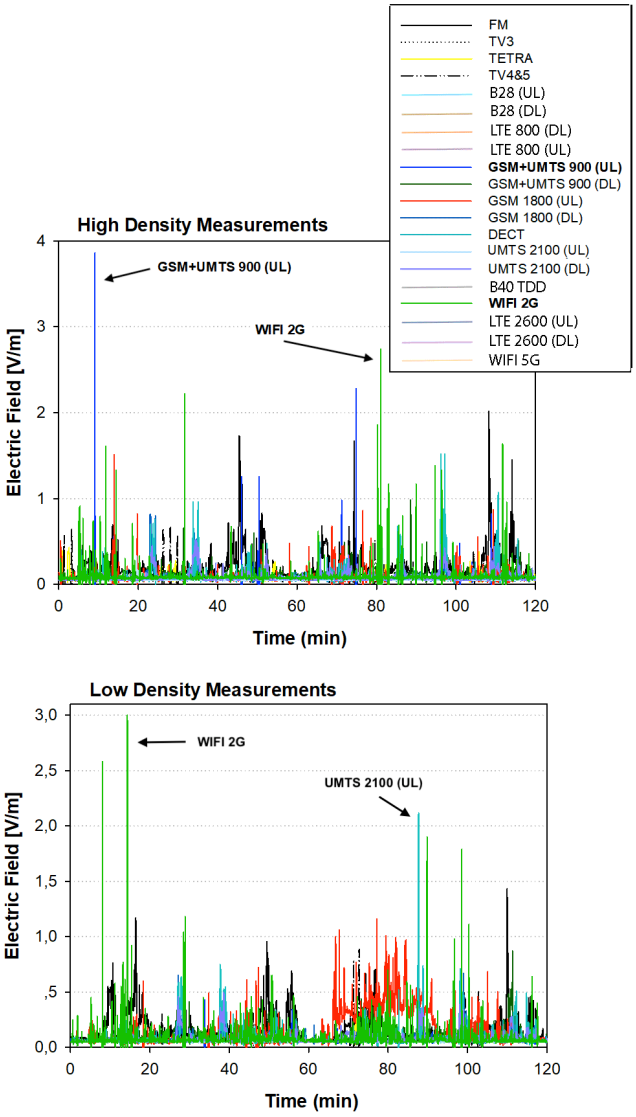

FIGURE 17. Measurement results within the tram wagon car route in the city of Bilbao, Spain, by means of EME Spy Evolution personal dosimeter for the high-density users' case (up) and low-density users' case (down).

antenna factor as different antennas were used to cover all the analyzed frequency bands.

From the obtained results, measured using the spectrum analyzer, some interesting conclusions can be stated. As in the previous results, the same trend is observed with maximum exposure given by personal cellular communications and Wi-Fi systems. Conversely, in this time-interval case study, the highest values are obtained for the downlink (DL) connection: UMTS 2100 DL with a maximum of 1.2 V/m, followed by GSM/UMTS 900 DL with 0.19 V/m and GSM 1800 DL with 0.01 V/m. Finally, relevant exposition is recorded from WIFI 2G, with a maximum of 0.25 V/m. This exposure behavior is explained by the EMF exposure caused by the continuous base station DL monitoring (continuous transmission) in order to detect and capture the beacon from potential users' handsets. In this sense, there were no

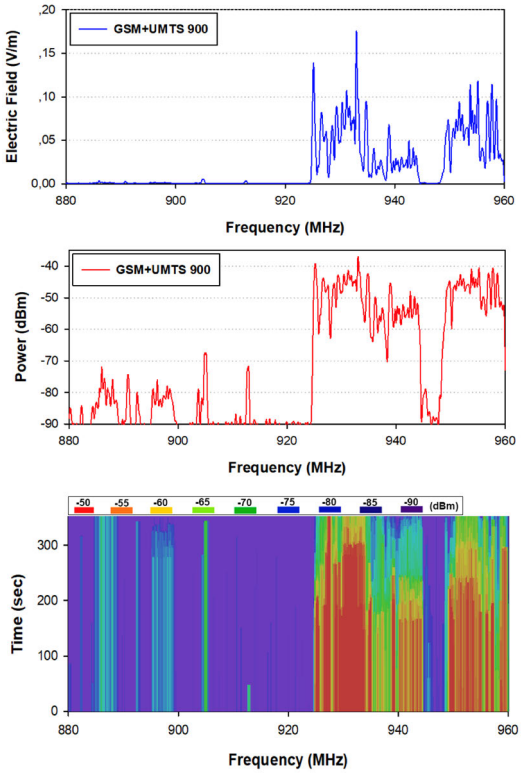

FIGURE 18. Measurement results within the tram wagon car by means of the spectrum analyzer for the GSM/UMTS 900 frequency band: E-field values (up), Power values (middle) and spectrogram (bottom).

other passengers stablishing up-link connections during the recorded time intervals. In general, passive DL exposure is further down the potential active exposure caused by up-link connections, in terms of RF-EMF radiation exposure assessment.

For both measurement approaches in realistic-case conditions, all the obtained E-field exposure levels are far below the current international limits, thus, verifying compliance with current EMF legislation (1-2% of the lowest reference levels provided by ICNIRP guidelines for the corresponding frequency band (41.25 V/m – 61 V/m)).

In summary, it can be concluded that the spectrum analyzer results (static approach) are more accurate than PEM measurements (dynamic approach) due to a continuous EMF exposure monitoring avoiding the PEM's sample interval (5 second in this case), which can lead to miss relevant levels. However, PEM measurements are easier to perform in terms of equipment cost, staff training, dynamic environments and measurements in long intervals of time. So, the election of the measurement campaign methodology must be determined by the features of the scenario under analysis as well as the accuracy, time and type of exposure assessment needed.

E. RAY LAUNCHING VALIDATION

As it has been previously introduced in Section III.A, a controlled measurement campaign has been performed within the tram wagon car, in order to validate the proposed simulation algorithm. In Fig. 22, the measurement campaign spatial

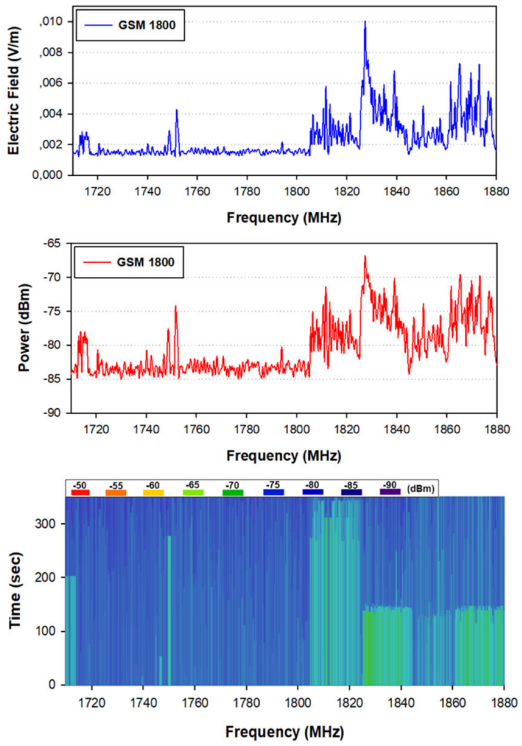

FIGURE 19. Measurement results within the tram wagon car by means of the spectrum analyzer for the GSM 1800 frequency band: E-field values (up), Power values (middle) and spectrogram (bottom).

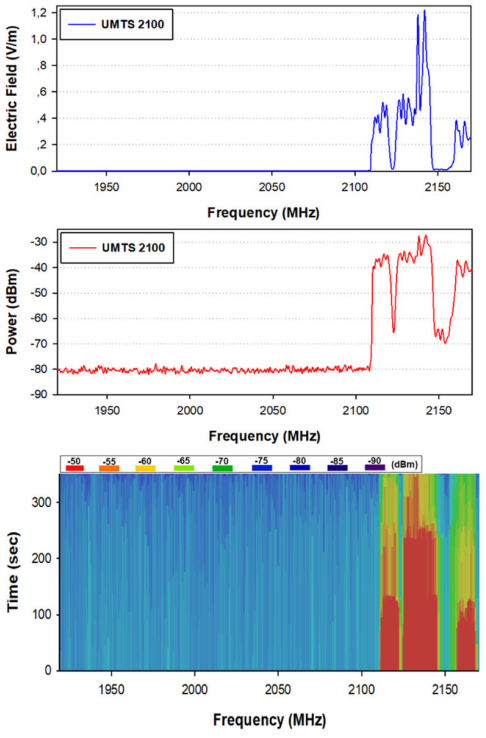

FIGURE 20. Measurement results within the tram wagon car by means of the spectrum analyzer for the UMTS 2100 frequency band: E-field values (up), Power values (middle) and spectrogram (bottom).

design is depicted showing the location of the transmitter as well as the measurement points along the complete volume of the simulated tram wagon car model. In the central

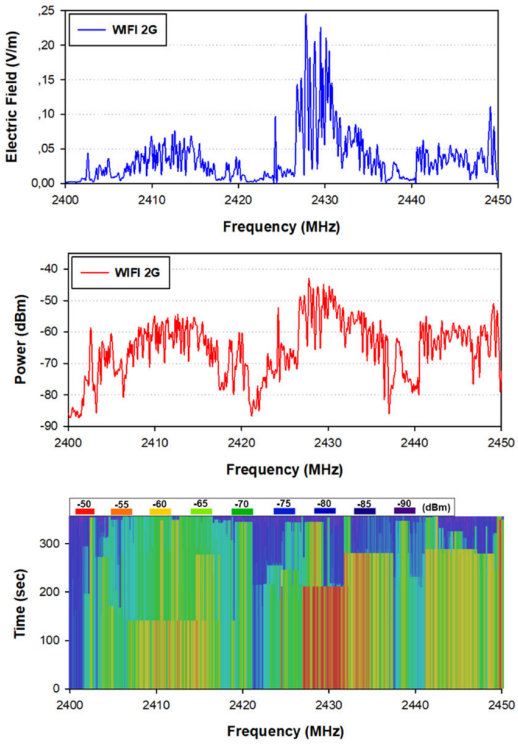

FIGURE 21. Measurement results within the tram wagon car by means of the spectrum analyzer for the WIFI 2G frequency band: E-field values (up), Power values (middle) and spectrogram (bottom).

line, measurements have been taken at a height of 1.1 m and conversely, the receiver locations have been established just above the seats, for the lateral measurements. A summary of the controlled measurement campaign specifications, including the followed procedure and the specific parameters and hardware equipment used, is presented for reference in Section III.A.

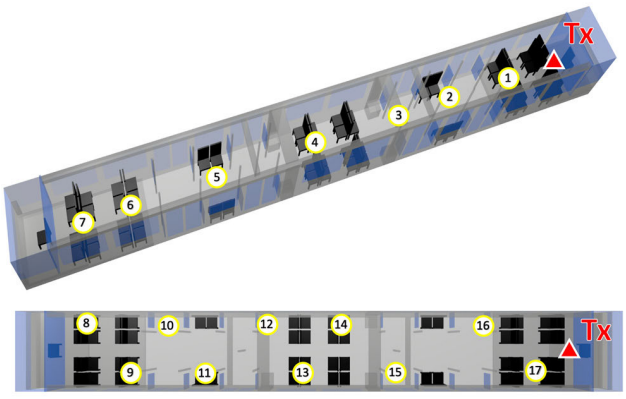

FIGURE 22. Transmitter and measurement points in the controlled measurement campaign within the tram wagon.

For the same measurement points, simulated E-field exposure levels have been calculated from the corresponding 3D mesh cuboids, in which the simulated scenario has been divided. Fig. 23 shows the comparison between the

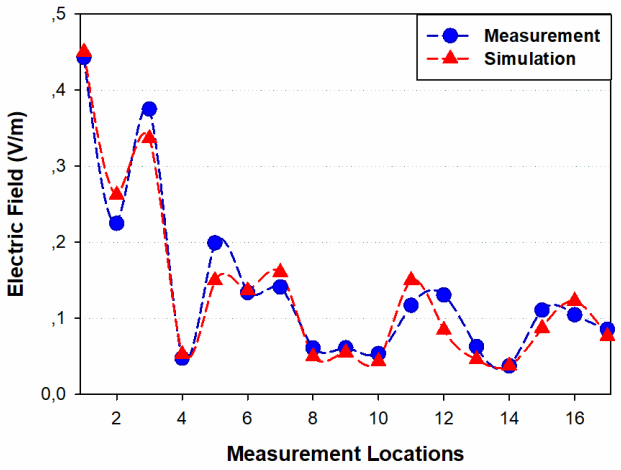

FIGURE 23. Comparison between simulation and measurement results, within the tram wagon car.

simulation and measurement results as a function of location within the tram wagon car. Analyzing the obtained graph, good agreement is achieved between simulation and experimental measurements, with a mean error of 0.019 V/m. Thus, allowing validation of the proposed simulation technique for non-ionizing radiation exposure assessment in complex heterogeneous indoor environments, as the tram wagon car.

V. CONCLUSION

This work presents a complete E-field strength distribution spatial characterization within public transportation trams, considering different cellular systems and user densities in realistic-case conditions, applicable to dosimetric estimation and analysis. By means of an in-house developed deterministic 3D-RL algorithm, E-field exposure estimations have been obtained for the complete volume of the tram wagon car. This simulation approach allows the assessment of the tram's indoor distribution impact in terms of topology and morphology as well as considering its different materials properties.

The user mobile phone base station up-link has been assessed considering different cellular communication systems (from 2G to 5G) in the corresponding frequency bands, including 5G NR FR1 and FR2. Special emphasis has been made in the E-field exposure analysis given by the influence of users' densities and their corresponding body shielding effects in the proximity of the transmitting antenna. In this sense, two different areas have been defined: impact and remote area, showing the highest E-field distribution values concentrated around the transmitter antenna (impact area), determined in a range of 2 – 2.5 m approximately, depending on the frequency band under analysis. Nevertheless, despite the high number of sources (2G/3G/4G/5G and Wi-Fi) involved, both measurements and simulations show field strength levels far below the maximum limits established by the ICNIRP guidance (1-2% of the aforementioned limits).

For the 5G case, the impact on the potential use of beamforming techniques in the mobile handsets has been considered, showing that body shielding of nearby users seriously affect signal propagation. Specifically, this effect is intensified for the high-density case and particularly in the mm-wave frequency range. In addition, RF-EMF radiation exposure average within the complete volume of the tram is lower when considering directive antennas in the mobile handset rather than omni-directional. However, users located within the antenna beam communication link, will suffer an average E-field exposure increase of 74% more than in an omni-directional mobile handset system. Thus, when considering future 5G cellular systems with directive antennas at the UE within public crowded indoor scenarios such as the presented in urban transportation vehicles, the probability of having users within an antenna beam is higher, so the local EMF radiation exposure will also be higher compared with current cellular systems. Overall, with a completely 5G system implemented and widely used within an indoor scenario, it can be predicted that RF-EMF radiation exposure average (specially for brief or irregular local exposure) can be higher in the worst-case scenario, yet remaining far below the aforementioned maximum limits.

In order to provide clear EMF insight, a complete E-field measurements campaign has been performed in a real tram wagon car with both, a PEM device and a spectrum analyzer. Comparison results evidence the differences between both methodologies in terms of simplicity (PEM approach) and results accuracy (spectrum analyzer approach). By means of a controlled campaign of measurements, the proposed simulation methodology has been validated showing good agreement with the experimental measurements.

Results reveal the complexity of EMF exposure characterization in this type of vehicular scenarios, due to the significant impact of multipath propagation cause by the indoor design (dimensions, morphology and topology of the scenario), the users' densities involved, and especially the frequency under analysis. Moreover, simulation results show the considerable impact of user densities within the tram scenario, confirming the body shielding effect and the increase of E-field exposure levels in the vicinity of the transmitter antenna, being more intensified for the high-density cases and especially at high frequencies. Hence, a uniform passenger distribution is recommended during rush hours, to avoid or mitigate the concentration of possible EMF emitting sources and thus, reducing potential impact areas and average E-field levels.

The proposed simulation methodology can be a useful and suitable technique to satisfactorily assess and verify EMF exposure recommendations and limits and therefore implement safe, efficient and reliable 5G deployments for complex heterogeneous environments such as urban transportation systems.

REFERENCES

[1] D. A. Hensher, "Why is light rail starting to dominate bus rapid transit yet again?" *Transp. Rev.*, vol. 36, no. 3, pp. 289–292, Mar. 2016.

[2] D. Houston, A. Dang, J. Wu, Z. Chowdhury, and R. Edwards, "The cost of convenience; air pollution and noise on freeway and arterial light rail station platforms in los angeles," *Transp. Res. Part D, Transp. Environ.*, vol. 49, pp. 127–137, Dec. 2016.

[3] D. Pojani and D. Stead, "Policy design for sustainable urban transport in the global south," *Policy Design Pract.*, vol. 1, no. 2, pp. 90–102, Apr. 2018.

[4] (Oct. 2019). *The Global Tram and Light Rail Landscape, Statistics Brief prepared by the Rail Unit of the UITP Secretariat*. Brussels, Belgium. [Online]. Available: https://www.uitp.org/sites/default/files/cck-focus-papers-files/Statistics%20Brief%20-%20World%20LRT_web_1.pdf

[5] R. Buehler, J. Pucher, R. Gerike, and T. Götschi, "Reducing car dependence in the heart of europe: Lessons from Germany, Austria, and Switzerland," *Transp. Rev.*, vol. 37, no. 1, pp. 4–28, May 2016.

[6] S. Sagar, S. M. Adem, B. Struchen, S. P. Loughran, M. E. Brunjes, L. Arangua, M. A. Dalvie, R. J. Croft, M. Jerrett, J. M. Moskowitz, T. Kuo, and M. Röösli, "Comparison of radiofrequency electromagnetic field exposure levels in different everyday microenvironments in an international context," *Environ. Int.*, vol. 114, pp. 297–306, May 2018.

[7] S. Sagar, B. Struchen, V. Finta, M. Eeftens, and M. Röösli, "Use of portable exposimeters to monitor radiofrequency electromagnetic field exposure in the everyday environment," *Environ. Res.*, vol. 150, pp. 289–298, Oct. 2016.

[8] A. Thielens, M. Van den Bossche, C. Brzozek, C. R. Bhatt, M. J. Abramson, G. Benke, L. Martens, and W. Joseph, "Representativeness and repeatability of microenvironmental personal and head exposures to radio-frequency electromagnetic fields," *Environ. Res.*, vol. 162, pp. 81–96, Apr. 2018.

[9] K. Gryz and J. Karpowicz, "Radiofrequency electromagnetic radiation exposure inside the metro tube infrastructure in Warszawa," *Electromagn. Biol. Med.*, vol. 34, no. 3, pp. 265–273, Jul. 2015.

[10] S. Aerts, D. Plets, A. Thielens, L. Martens, and W. Joseph, "Impact of a small cell on the RF-EMF exposure in a train," *Int. J. Environ. Res. Public Health*, vol. 12, no. 3, pp. 2639–2652, Feb. 2015.

[11] D. Plets, S. Aerts, K. Vanhecke, W. Joseph, and L. Martens, "Comparison of uplink SAR values in train environment for different wireless technologies," in *Proc. IEEE Int. Symp. Antennas Propag. USNC/URSI Nat. Radio Sci. Meeting*, Jul. 2015, pp. 85–86.

[12] D. Plets, W. Joseph, S. Aerts, G. Vermeeren, N. Varsier, J. Wiart, and L. Martens, "Assessment of contribution of other users to own total whole-body RF absorption in train environment," *Bioelectromagnetics*, vol. 36, no. 8, pp. 597–602, Dec. 2015.

[13] M. Celaya-Echarri, L. Azpilicueta, P. Lopez-Iturri, E. Aguirre, S. De Miguel-Bilbao, V. Ramos, and F. Falcone, "Spatial characterization of personal RF-EMF exposure in public transportation buses," *IEEE Access*, vol. 7, pp. 33038–33054, 2019.

[14] I. C. N. I. R. P. Guideline, "Guidelines for limiting exposure to time-varying electric, magnetic, and electromagnetic fields (up to 300 GHz)," *Health Phys.*, vol. 75, no. 5, pp. 494–522, Apr. 1998.

[15] *IEEE Standard for Safety Levels With Respect to Human Exposure to Radio Frequency Electromagnetic Fields, 3 kHz to 300 GHz*, Standard C95.1, 2005.

[16] *IEEE Approved Draft Standard for Safety Levels With Respect to Human Exposure to Electric, Magnetic and Electromagnetic Fields, 0 Hz to 300 GHz*, Standard C95.1-2019, 2019.

[17] I. Commission on Non-Ionizing Radiation Protection (ICNIRP)1, "Guidelines for limiting exposure to electromagnetic fields (100 kHz to 300 GHz)," *Health Phys.*, vol. 118, no. 5, pp. 483–524, May 2020.

[18] H. Mazar, "EMF, new ICNIRP guidelines and IEEE C95.1-2019 standard: Differences and similarities," in *Proc. 4th Int. Conf., Electromagn. Field Future Telecommun.*, Warsaw, Poland, Dec. 2019.

[19] K. Zhao, Z. Ying, and S. He, "Human exposure to mmWave phased array antennas in mobile terminal for 5G mobile system," in *Proc. IEEE 81st Veh. Technol. Conf. (VTC Spring)*, May 2015, pp. 1–2.

[20] K. Zhao, Z. Ying, and S. He, "EMF exposure study concerning mmWave phased array in mobile devices for 5G communication," *IEEE Antennas Wireless Propag. Lett.*, vol. 15, pp. 1132–1135, 2016.

[21] *FCC Code of Federal Regulations*, FCC, Washington, DC, USA, 2010.

[22] B. Thors, D. Colombi, Z. Ying, T. Bolin, and C. Tornevik, "Exposure to RF EMF from array antennas in 5G mobile communication equipment," *IEEE Access*, vol. 4, pp. 7469–7478, 2016.

[23] D. Colombi, B. Thors, and C. Tornevik, "Implications of EMF exposure limits on output power levels for 5G devices above 6 GHz," *IEEE Antennas Wireless Propag. Lett.*, vol. 14, pp. 1247–1249, 2015.

[24] B. Xu, K. Zhao, Z. Ying, D. Sjoberg, W. He, and S. He, "Analysis of impacts of expected RF EMF exposure restrictions on peak EIRP of 5G user equipment at 28 GHz and 39 GHz bands," *IEEE Access*, vol. 7, pp. 20996–21005, 2019.

[25] D. Colombi, B. Thors, C. Tornevik, and Q. Balzano, "RF energy absorption by biological tissues in close proximity to millimeter-wave 5G wireless equipment," *IEEE Access*, vol. 6, pp. 4974–4981, 2018.

[26] D. J. Panagopoulos, "Comparing DNA damage induced by mobile telephony and other types of man-made electromagnetic fields," *Mutation Res./Rev. Mutation Res.*, vol. 781, pp. 53–62, Jul. 2019.

[27] M. Karaboytcheva, *Effects of 5G Wireless Communication on Human Health*. Brussels, Belgium: European Parliamentary Research Service, Mar. 2020.

[28] A. Di Ciaula, "Towards 5G communication systems: Are there health implications?" *Int. J. Hygiene Environ. Health*, vol. 221, no. 3, pp. 367–375, Apr. 2018.

[29] (Mar. 2020). *Review of Published Literature between 2008 and 2018 of Relevance to Radiofrequency Radiation and Cancer, U.S. Food & Drug Administration*. [Online]. Available: https://www.fda.gov/media/135043/download

[30] Simkó and Mattsson, "5G wireless communication and health effects—A pragmatic review based on available studies regarding 6 to 100 GHz," *Int. J. Environ. Res. Public Health*, vol. 16, no. 18, p. 3406, Sep. 2019.

[31] *World Cancer Report 2020—Cancer Research for Cancer Prevention*, IARC/OMS, Lyon, France, 2020.

[32] World Health Organization (WHO). Fact Sheet 304. (May 2006). *Base Stations and Wireless Technology*. [Online]. Available: http://www.who.int/peh-emf/publications/factsheets/en/

[33] D. Urbinello, A. Huss, J. Beekhuizen, R. Vermeulen, and M. Röösli, "Use of portable exposure meters for comparing mobile phone base station radiation in different types of areas in the cities of basel and amsterdam," *Sci. Total Environ.*, vols. 468–469, pp. 1028–1033, Jan. 2014.

[34] R. Morimoto, A. Hirata, I. Laakso, M. C. Ziskin, and K. R. Foster, "Time constants for temperature elevation in human models exposed to dipole antennas and beams in the frequency range from 1 to 30 GHz," *Phys. Med. Biol.*, vol. 62, no. 5, pp. 1676–1699, Feb. 2017.

[35] S. Salous, *Radio Propagation Measurement and Channel Modelling*, 1st ed. London, U.K.: Wiley, 2013.

[36] S. Loredo, A. Rodriguez-Alonso, and R. P. Torres, "Indoor MIMO channel modeling by rigorous GO/UTD-based ray tracing," *IEEE Trans. Veh. Technol.*, vol. 57, no. 2, pp. 680–692, Mar. 2008.

[37] L. Azpilicueta, M. Rawat, K. Rawat, F. M. Ghannouchi, and F. Falcone, "A ray launching-neural network approach for radio wave propagation analysis in complex indoor environments," *IEEE Trans. Antennas Propag.*, vol. 62, no. 5, pp. 2777–2786, May 2014.

[38] L. Azpilicueta, F. Falcone, and R. Janaswamy, "A hybrid ray launching-diffusion equation approach for propagation prediction in complex indoor environments," *IEEE Antennas Wireless Propag. Lett.*, vol. 16, pp. 214–217, 2017.

[39] F. Casino, L. Azpilicueta, P. Lopez-Iturri, E. Aguirre, F. Falcone, and A. Solanas, "Optimized wireless channel characterization in large complex environments by hybrid ray launching-collaborative filtering approach," *IEEE Antennas Wireless Propag. Lett.*, vol. 16, pp. 780–783, 2017.

[40] *Effect of Building Materials and Structures on Radiowave Propagation Above About 100 MHz*, document ITU-R P.2040-1, International Telecommunication Union Recommendation, 2015.

[41] E. Aguirre, J. Arpon, L. Azpilicueta, S. De Miguel Bilbao, V. Ramos, and F. J. Falcone, "Evaluation of electromagnetic dosimetry of wireless systems in complex indoor scenarios with human body interaction," *Prog. Electromagn. Res. B*, vol. 43, pp. 189–209, 2012.

[42] T. S. Rappaport, R. W. Heath Jr, R. C. Daniels, and J. N. Murdock, "Millimeter wave wireless communications," in *Communications Engineering and Emerging Technologies Series*. Upper Saddle River, NJ, USA: Prentice-Hall, 2015.

[43] Plan Nacional 5G 2018-20. (Mar. 2020). *Ministerio de Energía, Turismo y Avance Digital de España*. [Online]. Available: https://avancedigital.gob.es/5G/Documents/plan_nacional_5g.pdf

[44] *Power Density Simulation and Measurement Report*, FCC, Washington, DC, USA, Dec. 2018. [Online]. Available: https://fccid.io/IHDT56XL1/RF-Exposure-Info/PD-Simulation-report-0213-4170293

[45] Y. Huo, X. Dong, and W. Xu, "5G cellular user equipment: From theory to practical hardware design," *IEEE Access*, vol. 5, pp. 13992–14010, 2017.
[46] Y. Huo, X. Dong, W. Xu, and M. Yuen, "Cellular and WiFi co-design for 5G user equipment," in *Proc. IEEE 5G World Forum (5GWF)*, Jul. 2018, pp. 256–261.
[47] D. Liu, M. Zhang, B. Wang, and J. Wang, "An ultra-low-profile MIMO antenna for 5G smart-phones," in *Proc. Int. Symp. Antennas Propag. (ISAP), Busan, Korea (South)*, Oct. 2018, pp. 1–2.
[48] S. Xu, M. Zhang, X. Shi, D. Liu, H. Wen, and J. Wang, "Anisotropic metamaterial based decoupling strategy for MIMO antenna in mobile handsets," in *Proc. Int. Workshop Antenna Technol., Small Antennas, Innov. Struct., Appl. (iWAT)*, Mar. 2017, pp. 34–37.
[49] X. Shi, M. Zhang, S. Xu, D. Liu, H. Wen, and J. Wang, "Dual-band 8-element MIMO antenna with short neutral line for 5G mobile handset," in *Proc. 11th Eur. Conf. Antennas Propag. (EUCAP)*, Mar. 2017, pp. 3140–3142.
[50] D. Q. Liu, M. Zhang, H. J. Luo, H. L. Wen, and J. Wang, "Dual-band platform-free PIFA for 5G MIMO application of mobile devices," *IEEE Trans. Antennas Propag.*, vol. 66, no. 11, pp. 6328–6333, Nov. 2018.
[51] L. Azpilicueta, M. Rawat, K. Rawat, F. Ghannouchi, and F. Falcone, "Convergence analysis in deterministic 3D ray launching radio channel estimation in complex environments," *Appl. Comput. Electromagn. Soc. J.*, vol. 29, no. 4, pp. 256–271, 2014.
[52] L. Azpilicueta, E. Aguirre, P. López-Iturri, and F. Falcone, "An accurate UTD extension to a ray-launching algorithm for the analysis of complex indoor radio environments," *J. Electromagn. Waves Appl.*, vol. 30, no. 1, pp. 43–60, Jan. 2016.
[53] E. Chiaramello, M. Bonato, S. Fiocchi, G. Tognola, M. Parazzini, P. Ravazzani, and J. Wiart, "Radio frequency electromagnetic fields exposure assessment in indoor environments: A review," *Int. J. Environ. Res. Public Health*, vol. 16, no. 6, p. 955, Mar. 2019.
[54] K. Foster and D. Colombi, "Thermal response of tissue to RF exposure from canonical dipoles at frequencies for future mobile communication systems," *Electron. Lett.*, vol. 53, no. 5, pp. 360–362, Mar. 2017.
[55] W. He, B. Xu, M. Gustafsson, Z. Ying, and S. He, "RF compliance study of temperature elevation in human head model around 28 GHz for 5G user equipment application: Simulation analysis," *IEEE Access*, vol. 6, pp. 830–838, 2018.
[56] F. T. Pachón-García, K. Fernández-Ortiz, and J. M. Paniagua-Sánchez, "Assessment of Wi-Fi radiation in indoor environments characterizing the time & space-varying electromagnetic fields," *Measurement*, vol. 63, pp. 309–321, Mar. 2015.
[57] M. Gallastegi, M. Guxens, A. Jiménez-Zabala, I. Calvente, M. Fernández, L. Birks, B. Struchen, M. Vrijheid, M. Estarlich, M. F. Fernández, M. Torrent, F. Ballester, J. J. Aurrekoetxea, J. Ibarluzea, D. Guerra, J. González, M. Röösli, and L. Santa-Marina, "Characterisation of exposure to non-ionising electromagnetic fields in the spanish INMA birth cohort: Study protocol," *BMC Public Health*, vol. 16, no. 1, p. 167, Feb. 2016.
[58] K. Karipidis, S. Henderson, D. Wijayasinghe, L. Tjong, and R. Tinker, "Exposure to radiofrequency electromagnetic fields from Wi-Fi in australian schools," *Radiat. Protection Dosimetry*, vol. 175, no. 4, pp. 432–439, 2017.
[59] J. F. B. Bolte, G. van der Zande, and J. Kamer, "Calibration and uncertainties in personal exposure measurements of radiofrequency electromagnetic fields," *Bioelectromagnetics*, vol. 32, no. 8, pp. 652–663, Dec. 2011.
[60] U. Knafl, H. Lehmann, and M. Riederer, "Electromagnetic field measurements using personal exposimeters," *Bioelectromagnetics*, vol. 29, no. 2, pp. 160–162, 2008.
[61] G. Neubauer, S. Cecil, W. Giczi, B. Petric, P. Preiner, J. Fröhlich, "Final report on the project C2006-07, evaluation of the correlation between RF dosimeter reading and real human exposure," Austrian Res. Centers GmbH, Seibersdorf, Austria, ARC-Report ARC-IT-0218, Apr. 2008.
[62] S. D. Miguel-Bilbao, J. Blas, J. Karpowicz, and V. Ramos, "Study of body position dependence on human exposure in the 2.4 GHz band," in *Proc. Int. Symp. Electromagn. Compat. EMC Eur.*, Sep. 2019, pp. 1112–1115.
[63] C. Bornkessel, M. Blettner, J. Breckenkamp, and G. Berg-Beckhoff, "Quality control for exposure assessment in epidemi- ological studies," *Radiat. Protection Dosimetry*, vol. 140, no. 3, pp. 287–293, 2010.
[64] O. Lauer, G. Neubauer, M. Röösli, M. Riederer, P. Frei, E. Mohler, and J. Fröhlich, "Measurement setup and protocol for characterizing and testing radio frequency personal exposure meters," *Bioelectromagnetics*, vol. 33, no. 1, pp. 75–85, Jan. 2012.

MIKEL CELAYA-ECHARRI (Graduate Student Member, IEEE) received the Computer Science Engineering Degree and the master's degree in project management from the Public University of Navarre (UPNA), Pamplona, Navarre, Spain, in 2011 and 2015, respectively. He is currently pursuing the Ph.D. degree in engineering of science with Tecnologico de Monterrey, Mexico. He has worked in different research projects at Tafco Metawireless S. L. (telecommunications company placed at Navarre). He was a Visiting Assistant with the Networks and Telecommunications Research Group, Tecnologico de Monterrey, from 2015 to 2017. His research interests include wireless sensor networks, radiopropagation, dosimetric analysis, project management, and computer science.

LEYRE AZPILICUETA (Senior Member, IEEE) received the Telecommunications Engineering Degree, the master's degree in communications, and the Ph.D. degree in telecommunication technologies from the Public University of Navarre (UPNa), Spain, in 2009, 2011, and 2015, respectively. In 2010, she has worked as a Radio Engineer with the Research and Development Department, RFID Osés. She is currently working as an Associate Professor and a Researcher with Tecnologico de Monterrey, Campus Monterrey, Mexico. She has over 150 contributions in relevant journals and conference publications. Her research interests include radio propagation, mobile radio systems, wireless sensor networks, ray tracing, and channel modeling. She was a recipient of the IEEE Antennas and Propagation Society Doctoral Research Award 2014, the Young Professors and Researchers Santander Universities 2014 Mobility Award, the ECSA 2014 Best Paper Award, the IISA 2015 Best Paper Award, the Best Ph.D., in 2016, awarded by the Colegio Oficial de Ingenieros de Telecomunicación, the N2Women: Rising Stars in Computer Networking and Communications 2018 Award, the ISSI 2019 Best Paper Award, and the Junior Research Raj Mittra Travel Grant 2020.

JOLANTA KARPOWICZ received the Medical and Nuclear Electronic Master and Engineering Degree from the Warsaw Technical University, Poland, in 1991, and the Ph.D. degree in environmental engineering from the Central Institute for Labour Protection, Warszawa, Poland, in 2004. She is currently a Researcher and the Head of the Bioelectromagnetics Department, Central Institute for Labour Protection (accredited in evaluation of electromagnetic field and calibration of measurement devices). Her research interests include electromagnetic environment and influence on humans and electromagnetic field exposure related environmental safety, focused mainly on the workers safety-measurements, numerical modeling, safety standardization and legislation, and education. She is a member of BEMS, EBEA, ICES, and ICOH. She was an Expert in electromagnetic hazards at work to the European Council, the European Commission, and The Ministry of Labour, Poland.

VICTORIA RAMOS (Senior Member, IEEE) received the Ph.D. degree in biomedical engineering and telemedicine from the University of Alcala, Madrid, Spain, in 2005. She was a Telecommunications Engineer with the Polytechnic University of Madrid. From 1985 to 1996, she has worked as a Radio Communications Research and Development Engineer in the private industry. Since 1996, she has been a Research Scientist with the Instituto de Salud Carlos III, where she is currently a Ph.D. Researcher, and a Civil Servant, belonging to the Ministry of Science, Innovation and University, in the research area of telemedicine and e-health, Madrid. Her research interests include wireless communications applications for home care and the next generations of sensors networks and body area networks and telemedicine applications. Her objectives are to provide health care for mobile citizens and e-health focusing on new emergent health services based on telemedicine. It involves standards related to human exposure, medical devices immunity and radio communication EMC. She is the author or has coauthored of several books as well as of several articles for scientific congresses. She takes part of several Spanish Standardizations Committees.

PEIO LOPEZ-ITURRI (Member, IEEE) received the degree in telecommunications engineering, the master's degree in communications, and the Ph.D. degree in communication engineering from the Public University of Navarre (UPNA), Pamplona, Navarre, in 2011, 2012, and 2017, respectively. He has worked in ten different public and privately funded research projects. Since 2019, he has been partly working as a Researcher for Tafco Metawireless. He is also affiliated with the Institute for Smart Cities (ISC), UPNA. He has more than 120 contributions in indexed international journals, book chapters, and conference contributions. His research interests include radio propagation, wireless sensor networks, electromagnetic dosimetry, modeling of radio interference sources, mobile radio systems, wireless power transfer, the IoT networks and devices, 5G communication systems, and EMI/EMC. He received the 2018 Best Spanish Ph.D. thesis in Smart Cities in CAEPIA 2018 (3rd prize), sponsored by the Spanish network on research for Smart Cities CI-RTI and Sensors (ISSN 1424-8220). He was a recipient the ECSA 2014 Best Paper Award, the IISA 2015 Best Paper Award, and the ISSI 2019 Best Paper Award.

FRANCISCO FALCONE (Senior Member, IEEE) received the degree in telecommunication engineering and the Ph.D. degree in communication engineering from the Universidad Pública de Navarra (UPNA), Spain, in 1999 and 2005, respectively. From February 1999 to April 2000, he was a Microwave Commissioning Engineer with Siemens-Italtel, deploying microwave access systems. From May 2000 to December 2008, he was a Radio Access Engineer with Telefónica Móviles, performing radio network planning and optimization tasks in mobile network deployment. In January 2009, as a co-founding member, he has been the Director of Tafco Metawireless, a spin-off company from UPNA, until May 2009. In parallel, he was an Assistant Lecturer with the Electrical and Electronic Engineering Department, UPNA, from February 2003 to May 2009. In June 2009, he becomes an Associate Professor with the EE Department, and the Department Head, from January 2012 to July 2018. From January 2018 to May 2018, he was a Visiting Professor with the Kuwait College of Science and Technology, Kuwait. He is also affiliated with the Institute for Smart Cities (ISC), UPNA, which hosts around 140 researchers. He is currently acting as the Head of the ICT Section. His research interests include computational electromagnetics applied to the analysis of complex electromagnetic scenarios, with a focus on the analysis, design, and implementation of heterogeneous wireless networks to enable context-aware environments. He has over 500 contributions in indexed international journals, book chapters, and conference contributions. He received the CST 2003 and CST 2005 Best Paper Award, the Ph.D. Award from the Colegio Oficial de Ingenieros de Telecomunicación (COIT), in 2006, the Doctoral Award UPNA, in 2010, the First Juan Gomez Peñalver Research Award from the Royal Academy of Engineering of Spain, in 2010, the XII Talgo Innovation Award 2012, the IEEE 2014 Best Paper Award, in 2014, the ECSA-3 Best Paper Award, in 2016, and the ECSA-4 Best Paper Award, in 2017.